10390 *Inorg. Chem.* **2010**, *49*, 10390–10399
DOI: 10.1021/ic1014863

Inorganic Chemistry
Article

Magnetic Behavior Control in Niccolite Structural Metal Formate Frameworks $[NH_2(CH_3)_2][Fe^{III}M^{II}(HCOO)_6]$ (M = Fe, Mn, and Co) by Varying the Divalent Metal Ions

Jiong-Peng Zhao,[†] Bo-Wen Hu,[†] Francesc Lloret,[‡] Jun Tao,[§] Qian Yang,[†] Xiao-Feng Zhang,[†] and Xian-He Bu*,[†]

[†]*Department of Chemistry, and TKL of Metal and Molecule-Based Material Chemistry, Nankai University, Tianjin 300071, China,* [‡]*Instituto de Ciencia Molecular (ICMol), Universidad de Valencia, Polígono de La Coma, s/n, 46980-Paterna, Valencia, Spain, and* [§]*State Key Laboratory for Physical Chemistry of Solid Surfaces, Xiamen University, Xiamen 361005, China*

Received July 25, 2010

By changing template cation but introducing trivalent iron ions in the known niccolite structural metal formate frameworks, three complexes formulated $[NH_2(CH_3)_2][Fe^{III}M^{II}(HCOO)_6]$ (M = Fe for **1**, Mn for **2**, and Co for **3**) were synthesized and magnetically characterized. The variation in the compositions of the complexes leads to three different complexes: mixed-valent complex **1**, heterometallic but with the same spin state complex **2**, and heterometallic heterospin complex **3**. The magnetic behaviors are closely related to the divalent metal ions used. Complex **1** exhibits negative magnetization assigned as Néel *N*-Type ferrimagnet, with an asymmetric magnetization reversal in the hysteresis loop, and complex **2** is an antiferromagnet with small spin canting ($\alpha_{canting} \approx 0.06°$ and $T_{canting} = 35$ K), while complex **3** is a ferrimagnet with $T_N = 32$ K.

Introduction

In the past few decades, the design and synthesis of molecule magnetic materials have become the focus of intense research activities.[1] One of the most remarkable features of molecule based materials is that the magnetic properties may be altered by quite small and subtle variations in the level of molecular chemistry.[2] Materials with particular magnetic behavior could be designed by taking into account two important aspects: the spin carriers and the bridges.[3] However, arranging selected metal ions bridged by particular ligands in the crystal lattice is still a big challenge for chemists. Besides the metal ions and ligands, some factors govern the final structures and affect their magnetism such as the template, the pH value, the cations or anions for charge balance, and so on.[4] Among the plentiful magnetic molecules, the iron based complexes are still attractive as before.[5] The iron that has multivalencies and different spin states in the given coordination environment is a good candidate for design and synthesis of a molecule magnet.[5,6] Furthermore, in iron involved heterometallic system the magnetic behaviors will be more diverse and can be transformed by varying the spin carriers.[7]

*To whom correspondence should be addressed. E-mail: buxh@nankai.edu.cn. Fax: +86-22-23502458. Phone: +86-22-23502809.

(1) For examples: (a) Turnbull, M. M.; Sugimoto, T.; Thompson, L. K. *Molecule-Based Magnetic Materials*; American Chemical Society: Washington, DC, 1996. (b) Kahn, O. *Molecular Magnetism*; VCH: Weinheim, Germany, 1993. (c) Miller, J. S.; Drillon, M. *Magnetism: Molecules to Materials*; Wiley-VCH: Weinheim, 2001−2005. (d) Coronado, E.; Dunbar, K. R. *Inorg. Chem.* **2009**, *48*, 3293. (e) Zeng, Y.-F.; Hu, X.; Liu, F.-C.; Bu, X.-H. *Chem. Soc. Rev.* **2009**, *38*, 469.

(2) (a) Kahn, O., Ed.; *Magnetism Supramolecular Function*; Kluwer Academic Publishers: Dordrecht The Netherlands, 1996. (b) Nuttall, C. J.; Day, P. *Chem. Mater.* **1998**, *10*, 3050.

(3) Paredes-García, V.; Vega, V.; Novak, M. A.; Vaz, M. G. F.; Souza, D. A.; Venegas-Yazigi, D.; Spodine, E. *Inorg. Chem.* **2009**, *48*, 4737.

(4) (a) Yang, Y.-F.; Ma, Y.-S.; Guo, L.-R.; Zheng, L.-M. *Cryst. Growth Des.* **2008**, *8*, 1213. (b) Akutagawa, T.; Sato, D.; Koshinaka, H.; Aonuma, M.; Noro, S.; Takeda, S.; Nakamura, T. *Inorg. Chem.* **2008**, *47*, 5951. (c) Hayashi, H.; Karasawa, S.; Koga, N. *J. Org. Chem.* **2008**, *73*, 8683. (d) Song, H.-H.; Zheng, L.-M.; Lin, C.-H.; Wang, S.-L.; Xin, X.-Q.; Gao., S. *Chem. Mater.* **1999**, *11*, 2382. (e) Liu, F.-C.; Zeng, Y.-F.; Zhao, J.-P.; Hu, B.-W.; Sanudo, E. C.; Ribas, J.; Bu, X.-H. *Inorg. Chem.* **2007**, *46*, 7698.

(5) (a) Buser, H. J.; Schwarzenbach, D.; Petter, W.; Ludi, A. *Inorg. Chem.* **1977**, *16*, 2704. (b) Dunbar, K. R.; Heintz, R. A. *Prog. Inorg. Chem.* **1997**, *45*, 283. (c) Halder, G. J.; Kepert, C. J.; Moubaraki, B.; Murray, K. S.; Cashion, J. D. *Science* **2002**, *298*, 1762. (d) Lytvynenko, A. S.; Kolotilov, S. V.; Cador, O.; Gavrilenko, K. S.; Golhen, S.; Ouahab, L.; Pavlishchuk, V. V. *Dalton Trans.* **2009**, 3503. (e) Zheng, Y.-Z.; Xue, W.; Zhang, W.-X.; Tong, M.-L.; Chen, X.-M.; Grandjean, F.; Long, G. J.; Ng, S.-W.; Panissod, P.; Drillon, M. *Inorg. Chem.* **2009**, *48*, 2028.

(6) (a) Mandal, S.; Natarajan, S.; Grenèche, J.-M.; Riou-Cavellec, M.; Férey, G. *Chem. Mater.* **2002**, *14*, 3751. (b) Tian, Y.-Q.; Yao, S.-Y.; Guo, Y.-J.; Song, Y.; Zhang, G. *Chin. J. Inorg. Chem.* **2010**, *26*, 385–390. (c) Behera, J. N.; Rao, C. N. R. *Chem. Asian J.* **2006**, *1*, 742. (d) Zheng, Y.-Z.; Tong, M.-L.; Xue, W.; Zhang, W.-X.; Chen, X.-M.; Grandjean, F.; Long, G. J. *Inorg. Chem.* **2008**, *47*, 4077.

(7) (a) Agustí, G.; Carmen, M.. M.; Gaspar, A. B.; Real, J. A. *Inorg. Chem.* **2009**, *48*, 3371. (b) Lescoue1zec, R.; Vaissermann, J.; Toma, L. M.; Carrasco, R.; Lloret, F.; Julve, M. *Inorg. Chem.* **2004**, *43*, 2234. (c) Toma, L. M.; Lescouëzec, R.; Lloret, F.; Julve, M.; Vaissermann, J.; Verdaguer, M. *Chem. Commun.* **2003**, 1850. (d) Watts, I. D.; Carling, S. G.; Day, P. *J. Chem. Soc., Dalton Trans.* **2002**, 1429. (e) Coronado, E.; Gómez-Garcla, C. J.; Nuez, A.; Romero, F. M.; Waerenborgh, J. C. *Chem. Mater.* **2006**, *18*, 2670.

Published on Web 10/11/2010

As the smallest carboxylate, formate anion, with multiple bridging modes, being able to mediate ferro- or antiferromagnetic coupling between metal ions in different situations was used extensively to assemble molecule magnetic materials.[8−11] Two kinds of anionic divalent metal formate frameworks with different templates have been reported, such as perovskite-ike structure $[NH_2(CH_3)_2^+][M^{II}(HCOO)_3^-]$ with univalent template[12] and niccolite structure $[CH_3NH_2(CH_2)_2NH_2CH_3^{2+}][M_2(HCOO)_6^{2-}]$ with divalent template.[13] The templates are more likely to take the role of charge balancer. Keeping that in mind, we attempted to construct the niccolite structure by using the univalent template but introducing a trivalent iron ion into the system. Fortunately, three trivalent iron based complexes $[NH_2(CH_3)_2][Fe^{III}M^{II}(HCOO)_6]$ (M = Fe for **1**, Mn for **2**, and Co for **3**) have been synthesized and characterized. Magnetic studies indicated that the magnetism of the complexes are altered by changing the spin pairs. Although complex **1** was characterized as a Néel *N*-Type ferrimagnet by Hagen et al.[14] obtained by different synthetic methods when the work was in process. However, we found a more remarkable character of asymmetric magnetization reversal in the hysteresis loop of **1** that is very rare in molecular-based magnets.[2b] To investigate the observed asymmetry in the hysteresis of **1** a detailed study of the magnetism on one single crystal was carried out. When the divalent iron ions were replaced by manganese(II) or cobalt(II) an antiferromagnet with small spin canting complex **2** and a soft ferrimagnet complex **3** were obtained respectively.

Experimental Section

Materials and Physical Measurements. All the chemicals used for synthesis are of analytical grade and commercially available and used as received. Elemental analyses (C, H, N) were performed on a Perkin-Elmer 240C analyzer. The metal elements Fe, Mn, and Co were detected by atomic absorption spectrometry (AAS) (Hitachi 180−80). The X-ray powder diffraction (XRPD) was recorded on a Rigaku D/Max-2500 diffractometer at 50 kV, 40 mA for a Cu-target tube and a graphite monochromator. Simulation of the XRPD spectra was carried out by the single-crystal data and diffraction-crystal module of the Mercury (Hg) program available free of charge via the Internet at http://www.iucr.org

Magnetic data were collected using crushed crystals or one single-crystal on Quantum Design MPMS-XL-7-SQUID magnetometers at Xianmen University and Universidad de Valencia. The data were corrected using Pascal's constants to calculate the diamagnetic susceptibility, and an experimental correction for the sample holder was applied. Single-crystals of about 1.9−5 mg were used to perform the magnetization measurements of **1**. The relation between the crystallographic axes and single-crystal's shape was established after determining the orientation matrix on a Rigaku SCXmini diffractometer.

Synthesis of Complexes. **$[NH_2(CH_3)_2][Fe^{III}Fe^{II}(HCOO)_6]$ (1).** A mixture of $FeCl_3 \cdot 6H_2O$ (1.5 mmol) in dimethylformamide (DMF) and formic acid (total 15 mL) (V/V 1:1) was sealed in a Teflon-lined stainless steel vessel, heated at 140 °C for 2 days under autogenous pressure, and then cooled to room temperature. Black crystals of **1** were harvested in about ∼50% yield based on $FeCl_3 \cdot 6H_2O$. IR spectra of **1**, see Supporting Information, Figure S1. Anal. Calcd for $C_8H_{14}Fe_2NO_{12}$ (%): C, 22.46; H, 3.30; N, 3.27; Fe, 26.10; Found (%). C, 22.27; H, 3.10; N, 3.52. AAS (%): Fe 25.98.

Big single crystals of **1** were obtained by the similar process mentioned above but with more reactant (2 mmol $FeCl_3 \cdot 6H_2O$) and reaction times (3.5 days).

$[NH_2(CH_3)_2][Fe^{III}Mn^{II}(HCOO)_6]$ (2). A mixture of $FeCl_3 \cdot 6H_2O$ (0.75 mmol) and $MnCl_2 \cdot 4H_2O$ (0.75 mmol) in DMF and formic acid 15 mL (V/V 1:1) was sealed in a Teflon-lined stainless steel vessel, heated at 140 °C for 2 days under autogenous pressure, and then cooled to room temperature. Dark yellow crystals of **2** were harvested in about ∼50% yield based on $MnCl_2 \cdot 4H_2O$. IR spectra of **2**, see the Supporting Information, Figure S1. Anal. Calcd for $C_8H_{14}FeMnNO_{12}$ (%): C, 22.50; H, 3.30; N, 3.28; Fe, 13.08; Mn, 12.87. Found(%). C, 22.09; H, 3.20; N, 3.48; AAS (%): Fe, 12.97; Mn, 12.99, ratio of Fe: M_n = 0.98: 1.00.

$[NH_2(CH_3)_2][Fe^{III}Co^{II}(HCOO)_6]$ (3). A mixture of $FeCl_3 \cdot 6H_2O$ (0.75 mmol) and $CoCl_2 \cdot 6H_2O$ (0.75 mmol) in DMF and formic acid 15 mL (V/V 1:1) was sealed in a Teflon-lined stainless steel vessel, heated at 140 °C for 2 days under autogenous pressure, and then cooled to room temperature. Dark red crystals of **3** were harvested in about ∼50% yield based on $CoCl_2 \cdot 6H_2O$. IR spectra of **3**, see the Supporting Information, Figure S1. Anal. Calcd for $C_8H_{14}FeCoNO_{12}$ (%): C, 22.30; H, 3.27; N, 3.25; Fe, 12.96; Co, 13.67; Found (%). C, 22.57; H, 3.13; N, 3.26; AAS (%): Fe, 13.11, Co 13.58, ratio of Fe: Co = 1.02: 1.00.

X-ray Data Collection and Structure Determinations. X-ray single-crystal diffraction data for complexes **1**−**3** were collected on a Rigaku diffractometer at 293(2) K or 113(2) K with Mo−Kα radiation (λ = 0.71073 Å) by ω scan mode. The program SAINT[15] was used for integration of the diffraction profiles. All the structures were solved by direct methods using the SHELXS program of the SHELXTL package and refined by full-matrix least-squares methods with SHELXL (semiempirical absorption corrections were applied using SADABS program).[16] Metal atoms in each complex were located from the *E*-maps and other non-hydrogen atoms were located in successive difference Fourier syntheses and refined with anisotropic thermal parameters on F^2. The hydrogen atoms of the ligands were generated theoretically onto the specific atoms and refined isotropically with fixed thermal factors. Detailed crystallographic data are summarized in Table 1.

Results and Discussion

Description of Crystal Structure. The three complexes are isomorphic, and the structure contains one unique formate anion that bridges two metal ions Fe^{III} and M^{II} in *anti-anti* mode (see Figure 1a), to form a 3D framework, with one unique Me_2NH_2 that is disordered and came from the decomposition of the DMF[12] filled in the cavities of the structure (see Figure 1b). The metal ions are all in octahedral

(8) (a) Wang, X. Y.; Wang, Z. M.; Gao, S. *Chem. Commun.* **2007**, 1127. (b) Wang, Z. M.; Zhang, B.; Fujiwara, H.; Kobayashi, H.; Kurmoo, M. *Chem. Commun.* **2003**, 416. (c) Liu, T.; Zhang, Y. Z.; Wang, Z. M.; Gao, S. *J. Am. Chem. Soc.* **2008**, *130*, 10500. (d) Wang, X. Y.; Wang, Z. M.; Gao, S. *Chem. Commun.* **2008**, 281, and references cited therein.

(9) (a) Viertelhaus, M.; Henke, H.; Anson, C. E.; Powell, A. K. *Eur. J. Inorg. Chem.* **2003**, *44*, 2283. (b) Wang, X. Y.; Wei, H. Y.; Wang, Z. M.; Chen, Z. D.; Gao, S. *Inorg. Chem.* **2005**, 572. (c) Viertelhaus, M.; Adler, P.; Clérac, R.; Anson, C. E.; Powell, A. K. *Eur. J. Inorg. Chem.* **2005**, 692. (d) Wang, Z. m.; Zhang, B.; Otsuka, K.; Inoue, K.; Kobayashi, H.; Kurmood, M. *Dalton Trans.* **2004**, 2209.

(10) (a) Cornia, A.; Caneschi, A.; Dapporto, P.; Fabretti, A. C.; Gatteschi, D.; Malavasi, W.; Sangregorio, C.; Sessoli, R. *Angew. Chem., Int. Ed.* **1999**, *38*, 1780. (b) Manson, J. L.; Lancaster, T.; Chapon, L. C.; Blundell, S. J.; Schlueter, J. A.; Brooks, M. L.; Pratt, F. L.; Nygren, C. L.; Qualls, J. S. *Inorg. Chem.* **2005**, *44*, 989.

(11) Zhao, J.-P.; Hu, B.-W.; Yang, Q.; Hu, T.-L.; Bu, X.-H. *Inorg. Chem.* **2009**, *48*, 7111.

(12) Wang, X.-Y.; Gan, L.; Zhang, S.-W.; Gao, S. *Inorg. Chem.* **2004**, *43*, 4615.

(13) Wang, Z.-M.; Zhang, X.-Y.; Batten, S.-R.; Kurmoo, M.; Gao, S. *Inorg. Chem.* **2007**, *46*, 8439.

(14) Hagen, K. S.; Naik, S. G.; Huynh, B. H.; Masello, A.; Christou, G.. *J. Am. Chem. Soc.* **2009**, *131*, 7516.

(15) *SAINT Software Reference Manual*; Bruker AXS: Madison, WI, 1998.

(16) Sheldrick, G. M. *SHELXTL NT, Program for Solution and Refinement of Crystal Structures*, Version 5.1; University of Göttingen: Göttingen, Germany, 1997.

Table 1. Crystal Data and Structure Refinement Parameters for Complexes **1**, **2**, and **3**

	1 (293 K)	**1** (113 K)	**2**	**3**
chemical formula	$C_8H_{14}Fe_2NO_{12}$	$C_8H_{14}Fe_2NO_{12}$	$C_8H_{14}FeMnNO_{12}$	$C_8H_{14}FeCoNO_{12}$
formula weight	427.90	427.90	426.99	430.98
space group	$P\bar{3}1/c$	$P\bar{3}1/c$	$P\bar{3}1/c$	$P\bar{3}1/c$
a (Å)	8.2699(12)	8.2366(12)	8.3151(12)	8.2486(12)
b (Å)	8.2699(12)	8.2366(12)	8.3151(12)	8.2486(12)
c (Å)	13.930(3)	13.840(3)	14.001(3)	13.790(3)
V/Å^3	825.1(2)	813.2(2)	838.3(2)	812.6(2)
Z	2	2	2	2
D/g cm^{-3}	1.722	1.748	1.692	1.761
μ/mm^{-1}	1.816	1.842	1.675	1.972
T/K	293(2)	113(2)	293(2)	293(2)
R [a]/wR [b]	0.0317/0.0640	0.0403/0.0922	0.0395/0.0703	0.0324/0.0664

[a] $R = \sum||F_o| - |F_c||/\sum|F_o|$. [b] $R_w = [\sum w(F_o^2 - F_c^2)^2/\sum w(F_o^2)^2]^{1/2}$.

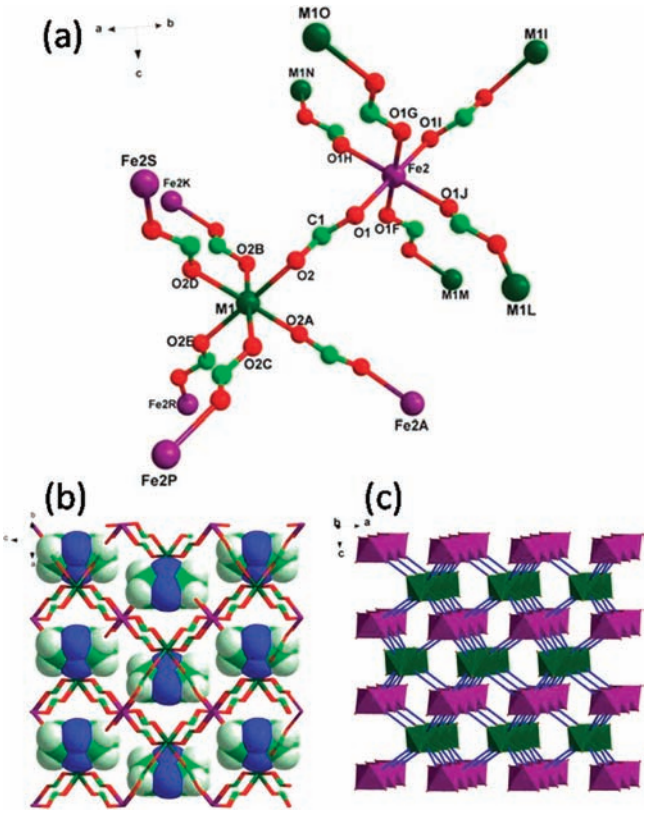

Figure 1. (a) Coordination and linkage modes of the ligands and metal ions in the complexes. (b) 3D space-filling view of the $[NH_2(CH_3)_2]$-$[Fe^{III}M^{II}(HCOO)_6]$ framework with the cations filled in the cavities. (c) Niccolite structural network topology of the complex with the two sublattices of the two types of metal ions in polyhedron views. Fe^{III} in purple, M^{II} in dark green, O in red, N in blue, and the cation H in white.

geometry coordinated by six oxygen atoms from six formate anions (see Figure 1a). The two independent metal atoms in the asymmetric unit were distinguished by the bond lengths. The Fe^{III}−O bonds lengths in the three complexes are in the range of 2.0093(13)−2.0208(15) Å, meanwhile the M^{II}−O bonds are in the range of 2.0825(15)−2.1621(16) Å. The M^{II}−O bond lengths decrease with the increase of the atomic number. The Fe^{II} ions in **1** came from the reduction of Fe^{III} by DMF during its oxidation to formate anion. The assignment of Fe^{III} and M^{II} ions (M = Fe, Mn, Co) were supported by bond valence calculations.[17] The detailed Bond Valence Sum (BVS) at 293 K calculations of M1 and Fe2 are as follows: for **1** Fe1(II) (2.08), Fe2(III) (3.05); for **2** Mn1(II) (2.19), Fe2(III) (3.03); for **3** Co1(II) (2.09), Fe2(III) (2.96). The key bond lengths and angles were summarized in Supporting Information, Table S1. Each Fe^{III} is connected to six M^{II} ions by six formate anions, and the M^{II} ions are all connected to six Fe^{III} ions. The $Fe^{III}\cdots M^{II}$ distances are 5.91, 5.94, and 5.88 Å for **1**,[14] **2**, and **3**, respectively. Thus the resulting framework is a binodal 6-connected niccolite network with $(4^{12}\cdot6^3)(4^9\cdot6^6)$ topology, in which M^{II} is the $(4^{12}\cdot6^3)$ node while Fe^{III} is the $(4^9\cdot6^6)$ node, and each node links only one node of the other type (see Figure 1c).[13] From the magnetic point the structures can be described as two sublattices containing Fe^{III} and M^{II} ions, respectively (see Figure 1c).[2b]

It is interesting that complex **1** is a mixed-valence complex, as Hagen's reported, complex **1** belongs to class II mixed-valence systems in the Robin−Day classification for the dark-purple color of **1** and the character of UV−vis spectrum.[14] To investigate the possibility of the electronic interaction between the oxidized and reduced sites in **1** we also resolved the crystal data in low temperature of 113 K and contrasted the diffraction data collected at 298 K, 173 K (reported by Hagen[14]), and 113 K. There is little difference in the Fe−O bond lengths in the same oxidized site in different temperature (at 298 K Fe1−O1 = 2.1245(14) Å, Fe2−O2 = 2.0093(9) Å; at 173 K Fe1−O1 = 2.1192(11) Å, Fe2−O2 = 2.0049(9) Å; at 113 K Fe1−O1 = 2.1180(15) Å, Fe2−O2 = 2.0067(13) Å). And the Fe1−Fe2 distances are about 5.909 Å, 5.889 Å, and 5.881 Å, respectively, at 298 K, 173 and 113 K, evidence a difference in the Fe−O bonds lengths between the two sites even in the low temperature of 113 K. That all suggests that a weak electronic interaction exists between the oxidized and reduced sites.

Magnetic Studies. Magnetic measurements were carried out on powder samples of complexes **1**, **2**, and **3** with their phase purity confirmed by XRPD (see Supporting Information, Figure S2). The obtained magnetic susceptibility data indicated that Fe^{III} and M^{II} are non-interacting at room temperature. However, with the decrease of the temperature they show different magnetic behaviors as discussed below, and so, they must be examined separately.

Compound 1: [$Fe^{III}Fe^{II}$]. Hagen et al. made this compound by a different route, and it shows *N*-Type ferrimagnetism that was confirmed by the temperature dependence of the $\chi_m T$ product measurement for the powder sample

(17) (a) Brown, I. D.; Altermatt, D. *Acta Crystallogr.* **1985**, *B41*, 244. (b) Brese, N. E.; O'Keeffe, M. *Acta Crystallogr.* **1991**, *B47*, 192. (c) Brown, I. D.; Gillespie, R. J.; Morgan, K. R.; Tun, Z.; Ummat, P. K. *Inorg. Chem.* **1984**, *23*, 4506.

of **1** (see the Supporting Information, Figure S3), and it was characterized more thoroughly for it was a novel spin system. The values of the best-fit parameters from the magnetic data under 0.2 T in the temperature 50−300 K through the Curie−Weiss law (Supporting Information, Figure S4a) are $\theta = -54.75$ K and $C = 7.83$ cm^3 K mol^{-1}, significantly above the spin-only one for one Fe^{III} and one Fe^{II} (ca. 7.375 cm^3 K mol^{-1}), indicating that the orbital contribution to the Fe^{II} moment must be taken into account.[18] The ferrimagnet state phase transition of **1** was confirmed by alternating current (*ac*) measurements. These measurements were carried out in the temperature range 25−44 K at 100 Hz (Supporting Information, Figure S5). Both in-phase and out-phase signals were observed with a peak at 37 K confirming the ferrimagnetic ordering at 37 K. Additional confirmation of this ordering was also demonstrated by heat capacity measurements which showed the occurrence of a λ-shape peak at 36.7 K both in the lack and in the presence of an applied direct current (*dc*) magnetic field (Supporting Information, Figure S6).

The observation of field-cooled-magnetization (FCM) with very large negative magnetization is very rare in molecular-based magnets and to our knowledge, Day and co-workers[2b,19] observed this behavior for the first time in a series of oxalato-bridged iron(II/III) two-dimensional compounds. However, several cases have been known for many years in the ferrites,[20] for example, in $NiFe_{2-x}V_xO_4$ where the concentration of magnetic ions on the tetrahedral (A) and octahedral (B) sites in the AB_2O_4 spinel lattice may vary as a result of forming solid solutions.

According to Néel's classic theory of ferrimagnets,[21] the ground state of a ferrimagnet is determined by the saturation magnetizations of each magnetic sublattice and their relative ordering rates with respect to temperature. So, a compensation temperature (T_{comp}) should occur in the magnetization when the magnetization of the two sublattices have different temperature dependencies and the sublattice with the smaller saturation magnetization initially orders more rapidly with decreasing temperature than the one with the larger saturation magnetization. In this sense, Néel[21] predicted the possibility that the spontaneous magnetization might change its sign below this T_{comp}, when the net magnetizations of the two sublattices cancel each other. These kinds of ferrimagnets were classified as *N*-Type ferrimagnets. Since the Fe^{III} ground state is orbitally non-degenerate, the magnetization of the Fe^{III} sublattice follows a Brillouin curve (with $S = 5/2$) in the molecular field approximation. However, Fe^{II} is orbitally degenerate, and it shows single-ion anisotropy because of spin−orbit coupling. So, the orientation of the Fe^{II} moments should exert the larger molecular field in the temperature range immediately below T_C.[22−24]

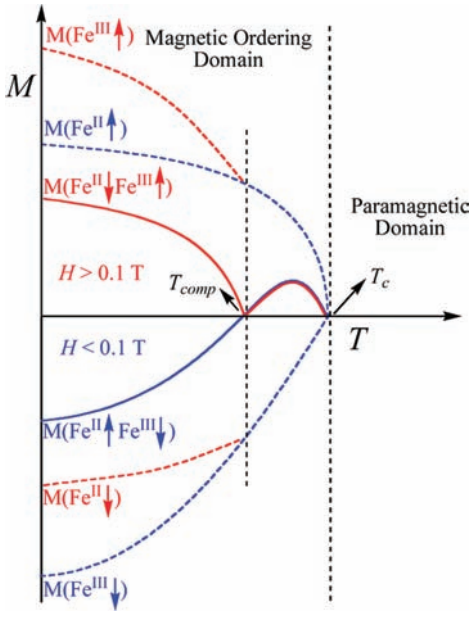

Figure 2. Temperature dependence of the magnetization for an *N*-Type Néel ferrimagnet containing Fe^{II} and Fe^{III}. The two magnetic sublattices ordering (dashed lines) and the resultant magnetization (solid lines) as a function of the applied magnetic field are shown.

Figure 2 illustrates two ways in which the magnetization for Néel *N*-Type ferrimagnets can vary with the temperature. In the solid blue line, the initial magnetic pole direction [Fe^{II}(parallel)-Fe^{III}(antiparallel)] is maintained and the magnetization becomes negative below T_{comp}, whereas the magnetization curve "bounces" in the solid red line as the magnetic pole reverses, that is, [Fe^{II}(parallel)-Fe^{III}(antiparallel)] changes to [Fe^{II}(antiparallel)-Fe^{III}(parallel)] below T_{comp} giving a positive magnetization at low temperatures. The magnetization in the temperature range between $T_C - T_{comp}$ is common for both cases. There is no energy barrier for the magnetic pole reversal in the molecular field approximation with fully isotropic exchange fields and so, the positive magnetization is thermodynamically favored over the negative one at low temperatures. Consequently, a positive magnetization would be expected as indicated by the solid red line. The occurrence of a negative magnetization (solid blue) for **1** below T_{comp} under magnetic fields lower than 0.1 T means that there is a barrier because of anisotropy which is sufficient to hinder the pole reversal. For applied fields greater than 0.1 T the magnetic energy is large enough to overcome this anisotropy (solid red line). The relative magnetic ordering of the Fe^{II} and Fe^{III} sublattices of **1** with respect to the applied dc field is shown in Figure 2 as dashed lines.

Interestingly, on the basis of Mössbauer spectroscopy measurements concerning the Fe^{II} and Fe^{III} sublattices in the layered oxalato-bridged Fe(II/III) compounds, Day and co-workers evidenced that they did not become magnetized to an equivalent extent at the same temperature and also that a more steeply increase of the magnetization of the Fe^{II} sublattice occurred below T_C versus that of the Fe^{III}.[19b]

(18) Figgis, B. N. *Introduction to Ligand Fields*; Interscience Publishers: New York, 1961.
(19) (a) Mathonière, C.; Nutall, C. J.; Carling, S. G.; Day, P. *Inorg. Chem.* **1996**, *35*, 1201. (b) Carling, G. C.; Day, P.; Nuttall, C. J. *Spectrochim. Acta* (*A*) **2001**, *57*, 1971.
(20) (a) Blasse, G.; Gorter, E. W. *J. Phys. Soc. Jpn. Sppl. B-1* **1962**, *17*, 176. (b) Gorter, E. W. *Philips Res. Rep.* **1954**, *9*, 403. (c) Goodenough, J. B. *Magnetism and the Chemical Bond*; Interscience: New York, 1963.
(21) Néel, L. *Ann. Phys.* (*Paris*) **1948**, *3*, 137–198.
(22) (a) Goodenough, J. B. *Phys. Rev.* **1968**, *171*, 466–479. (b) Menyuk, N.; Dwight, K.; Wickam, D. G. *Phys. Rev. Lett.* **1960**, *4*, 119. (c) Goodenough, J. B.; Nguyen, H. C. *C. R. Acad. Sci. Paris* **1994**, 319.
(23) Standley, K. J. *Oxide Magnetic Materials*; Clarendon Press: Oxford, 1962.
(24) Carlin, R. L. *Magnetochemistry*; Springer-Verlag: Berlin, 1986, 318.

Scheme 1

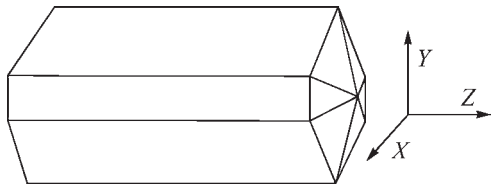

Another interesting magnetic feature of **1** is the asymmetric character of the hysteresis loop. This asymmetry can be seen in the Supporting Information, Figure S7 which corresponds to the hysteresis loop for a polycrystalline simple of **1** in the field range ±5 T at 2.0 K. The hysteresis loop is very asymmetric with significant shifts toward positive (or negative) fields. The shift depends on the sign of the applied field during the cooling process since the paramagnetic domain (T > 38 K) until the temperature where the magnetization is performed (that is, 2.0 K here). The hysteresis loop is shifted toward positive fields when the sample is cooled under a positive magnetic field whereas it is shifted toward negative fields when the cooling is carried out under a negative field (see Supporting Information, Figure S7). The value of the shift does not depend on the magnitude of the applied dc field in the cooling process, but only on its sign. The same loop is obtained by cooling under an applied field of 100 G or 5 T.

Additional magnetic measurements (hyteresis loop and FCM measurements) on single crystals of **1** were done to get a deeper understanding of the nature its magnetic behavior. Because of the space group is $P\bar{3}1/c$, the $\bar{3}$-fold axis of the trigonal lattice (that is the c axis) is necessarily one of the magnetic axes whereas the other two are in the ab plane which is perpendiculat to c.[24] As the single-crystal of **1** is prism-like, only its c axis could be distinctly recognized for orientation related to the magnetic field. The shape of the investigated single crystal of **1** is shown in Scheme 1 together with the definition of the arbitrary rotation axes. The Z axis corresponds to the c one whereas the other two are arbitrary and perpendicular to each other.

When the crystal is rotated around the Z axis (external magnetic field perpendicular to Z) and at temperatures below T_C, the values of the magnetization at any angle remain basically constant, evidencing that the X and Y are magnetically equivalent. The values of the magnetization largely vary under rotations around a perpendicular direction to Z (the c axis of the crystal), the maxima and minima occurring when the field is parallel (α = 180°) and perpendicular (α = 90°) to Z, respectively (see Supporting Information, Figure S8). So, the crystallographic c axis is the easy axis of the magnetization, and the perpendicular directions are identified as the hard ones.

The $M_{||}/M_{\perp}$ ratio between the parallel ($Z \parallel H$) and perpendicular values of the magnetization decreases when increasing the temperature, and it tends to one ($M_{||} \approx M_{\perp}$) as far as the temperature approaches the compensation point (T_{comp} = 29 K). At $T = T_{comp}$, $M_{||}/M_{\perp} < 1$ ($M_{||} < M_{\perp}$) because $M_{||}$ vanishes at such a temperature. At greater temperatures, the value of this ratio increases again. For $T > T_C$ the $M_{||}/M_{\perp}$ ratio tends to one.

The magnetization versus T plot for a single crystal with $Z \parallel H$ (easy axis of the magnetization) is shown in Figure 4. The open circles correspond to the FCM under an applied dc magnetic field of 100 G. As far as the temperature is decreased, the magnetization smoothly increases until 37.5 K. Below this temperature, it exhibits a sharp increase with a maximum at about 35 K and further decreases to vanish at the temperature of the compensation (T = 29 K). At $T < T_{comp}$, it becomes negative and attains the saturation around 5.0 K. These correspond to the Néel's predicted behavior for an N-Type ferrimagnet (see Figure 2). The magnetization of the Fe(III) and Fe(II) sublattices for each zone of the plot is shown in Figure 3, indicating its orientation with respect to the applied field as well as the relative magnitude of the two sublattices (relative size of the arrows). As indicated above, the magnetization of the Fe(II) sublattice increases faster than that of the Fe(III), in spite of the larger value of the saturation magnetization of the latter one. The triangles in Figure 3 correspond to the magnetization of the single crystal (same orientation) under warming since 2.0 to 40 K. Previously, the crystal was cooled from the paramagnetic region (T > 37 K) until 2 K under an applied dc field of 5 T. At 2.0 K the magnetic field is decreased from 5 T to 100 G and then, the magnetization measurements are performed by heating (the triangles are the experimental data). During the cooling process under 5 T, the orientations of the Fe(III) and Fe(II) sublattices are changed immediately after T_{comp} (29 K), resulting in a positive magnetization. If one disregards the sign of M, the two curves are totally similar (circles and triangles) until the crossing point corresponding to T_{comp}. Above this temperature, the magnetization becomes negative (antiparallel to the magnetic field) and a change of the orientation of the two sublattices occurs at 36 K (value of temperature very close to that of the magnetic ordering, $T \approx$ 37 K).

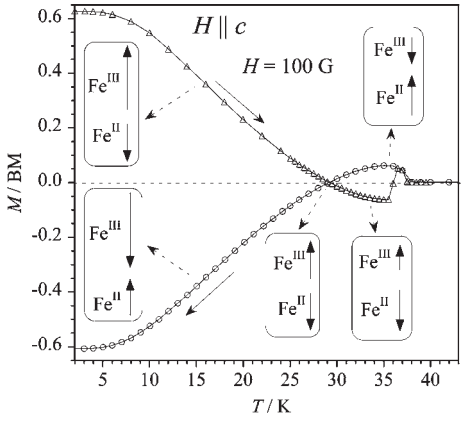

Figure 3. Temperature dependence of the magnetization of a crystal of **1** with $H \parallel Z$ and H = 100 G: (—○—) cooling-down; (—△—) warming after a FCM under 5 T. The inset schemes show the relative orientation of the Fe^{II} and Fe^{III} sublattices with respect to the applied magnetic field.

FCM measurements at 100 G for different values of the angle (α) between the Z axis and the applied dc field are shown in Figure 4. The magnetic field is parallel to Z for α = 180° (easy axis of the magnetization) whereas the hard axis corresponds to α = 90°. The effects of the magnetic field on the reorientation of the Fe(III) and Fe(II) sublattices are shown in the inset of Figure 4. The magnetic anisotropy precludes the reorientation of the sublattices for H < 0.1 T, leading to a negative magnetization. For H > 0.1 T and $T < T_{comp}$, one can see the reorientation of the Fe(III) and Fe(II) sublattices, as predicted by Néel for N-Type ferrimagnets.

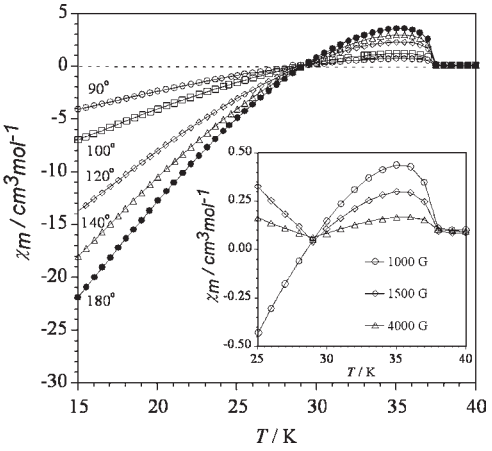

Figure 4. 100 G FCM for different orientations of a single crystal of **1**. α = 180° means $H \parallel Z$. The inset shows the FCM at different fields and $H \parallel Z$.

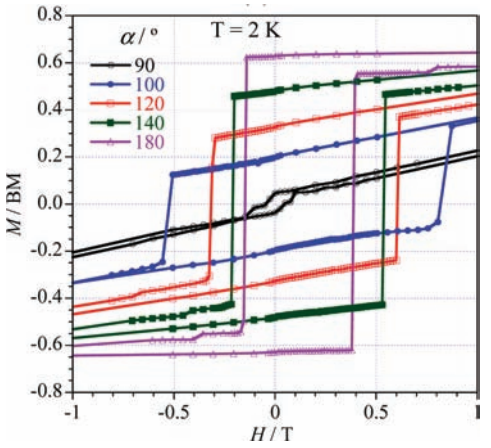

Figure 5. Detail of the central part of hysteresis loop at 2.0 K under different orientations of a single crystal of **1** [α = 180° is the easy axis ($H \parallel Z$) and α = 90° is the hard one ($H \perp Z$)].

To investigate the observed asymmetry in the hysteresis loop of the magnetization of the polycrystalline samples (see Supporting Information, Figure S7), the hysteresis loops of a single crystal were registered under different orientations with respect to the applied magnetic field and at several temperatures. The hysteresis loops at $T = 2.0$ K and different values of the angle between the magnetic field and the easy magnetization axis [α = 180° ($H \parallel Z$) and 90° ($H \perp Z$) are the easy and hard axes, respectively] are shown in Supporting Information, Figure S9. In this case, the crystal was cooled under a positive magnetic field ($H = +1$ T). A detail of the central part of that is given Figure 5. In the light of this figure, two relevant features deserves to be outlined: (i) the asymmetry of the hysteresis loop (shift toward positive fields) for any orientation of the single crystal, and (ii) the broadening of the cycle and the decrease of the remnant magnetization (M_R) when going from α = 180° (parallel) to α = 90° (perpendicular). The values of M_R and those of the coercive field at right (H_{c+}) and left (H_{c-}) branches are listed in Table 2. To quantify the shift of the hysteresis loop, we define the values of the shifted and average coercive fields as $H_i = (H_{c+} + H_{c-})/2$ and $H_c = (H_{c+} - H_{c-})/2$, respectively. The data listed in Table 2 show clearly how the average value of the coercive field increases when going from the easy axis to the hard one whereas that of the remnant magnetization decreases fast.

Table 2. Relevant Parameters of the Hysteresis Loop at $T = 2$ K Corresponding to Different Orientation of a Crystal of **1** (from Figure 5 and Supporting Information, Figure S9)

α/deg	H_{c-}/G	H_{c+}/G	M_R/BM	H_c/G	H_i/G
180	−1400	+3500	0.62	2450	1100
160	−1640	+4170	0.59	2905	1265
140	−2080	+5370	0.48	3725	1645
120	−3125	+6060	0.33	4593	1467
100	−5250	+8120	0.20	6735	1435
90	−450	+450	0.035	450	0

α = 180° is the easy axis, $H \parallel Z$, and α = 90° is the hard axis, $H \perp Z$.

Because of M_R tends to zero along the direction perpendicular, the arm of the magnetization for decreasing fields and that for the increasing ones appear as two parallel lines which are slightly shifted. Both branches do not converge at least until the maximum value of the applied magnetic field (5 T). A small hysteresis loop which occurs near to zero field could be due to a small misalignment of the crystal and/or some crystal defaults. The asymmetry of the loop after H_i is of the same order of magnitude and in the field range 1100−1645 G, although an apparent maximum of asymmetry occurs at an α value of about 140°.

The hysteresis loops of one single crystal oriented along the easy axis of magnetization (α = 180°) at different temperatures are shown in Figures 6a and 6b. The relevant magnetic parameters for the corresponding loops are listed Table 3. The values of M_R decrease with the temperature, and they practically vanish in the vicinity of the compensation temperature ($T = 29$ K), as expected. Above this temperature, they increase again and vanish for $T > T_C = 37$ K. In a similar manner, the coercive field (H_c) decreases with the temperature until the compensation point, and it increases again above this point and then vanishes at $T = 37$ K. It is interesting to note that the asymmetry of the loop after H_i decreases when the temperature increases, and it becomes symmetric for $T \geq 20$ K ($H_{int} = 0$).

The asymmetry observed in the magnetic hysteresis loop, that is, the shift to positive (or negative) fields, suggests that another magnetic field (H_i) is present in addition to the applied one (H_a). This field could act in competition with the applied external field H_a and then, the total energy of the magnetic crystal would be given by $-M(H_i + H_a)$. If H_i and H_a are collinear and in the same direction ($H = H_i + H_a$), the magnetic field acting on the crystal is greater than H_a, and the resulting magnetic moment of the Fe^{II} and Fe^{III} sublattices [$M = M(Fe^{III}) - M(Fe^{II})$], would be inverted at an applied field smaller than the coercive field expected in the absence of H_i. The opposite behavior occurs when H_i and H_a being collinear are in the opposite direction, $H = H_i - H_a$. In this case, the magnetic field acting on the crystal is smaller than H_a and the magnetic moment (M) is inverted at an applied field greater than the coercive field expected in the absence of H_i.

The magnetic moment (μ_i) responsible for the internal magnetic field (H_i) must be highly anisotropic, in such a way that when cooling the crystal under an applied magnetic field in the $+Z$ direction, since the paramagnetic region until $T < 20$ K, it remains oriented in the $+Z$ direction and the maximum applied field available in our SQUID (5 T) along the $-Z$ direction cannot invert the orientation of this magnetic moment. Assuming the occurrence of this magnetic moment, μ_i, the shift in the

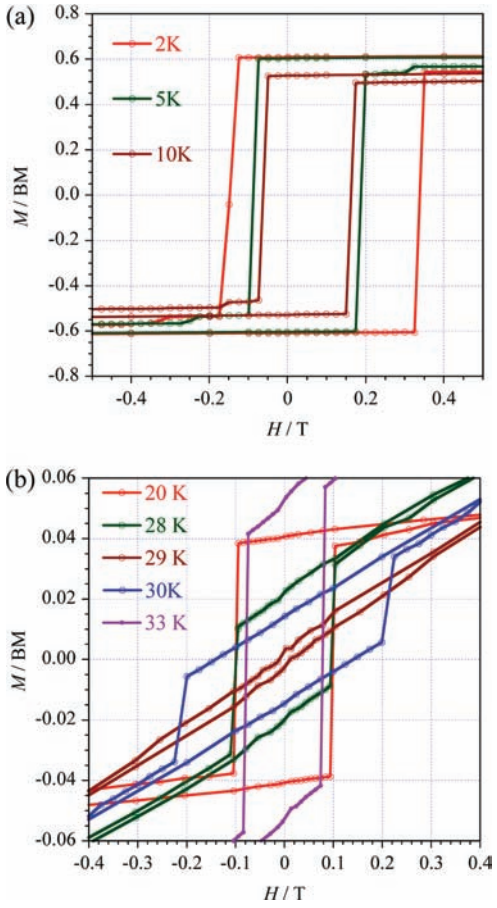

Figure 6. Hysteresis loop for a single crystal of **1** oriented with $H \parallel Z$ at different temperatures.

Table 3. Relevant Parameters of the Hysteresis Loop at Different Temperatures Corresponding to a Crystal of **1** with $H \parallel Z$ (from Figure 6)

T/K	H_{c-}/G	H_{c+}/G	M_R/BM	H_c/G	H_i/G
2	−1400	+3500	0.62	2450	1100
5	−900	+1900	0.60	1400	500
10	−650	+1600	0.53	1125	475
20	−1000	+1000	0.17	1000	0
28	−970	+970	0.021	970	0
29	−110	+110	0.0025	110	0
30	−1400	+1400	0.0014	1450	0
33	−780	+780	0.053	780	0

hysteresis loop can be understood as shown in Scheme 2, where the hysteresis loop is divided into four regions (A−D). If the crystal is magnetized in the $+Z$ direction, the internal magnetic moment (μ_i) provides a field in the opposed direction, $-Z$ (A). This means that μ_i and M interact antiferromagnetically. When the sign of the field is changed, both fields (H_a and H_i) are parallel and the magnetic moment [$M = M(Fe^{III}) - M(Fe^{II})$] experiences a field greater than H_a (B) and a coercive field smaller than that expected in the case where H_a were the only existing field (C). The reversal of μ_i does not occur for $H_a \leq 5$ T and $T < 20$ K, because of its large anisotropy. When going from C to D, the sign of H_a changes and M experiences a field smaller than H_a. Then, the coercive field is greater (it requires a greater H_a). The magnitude of μ_i has to be much smaller than that of $M = M(Fe^{III}) - M(Fe^{II})$ ($M \gg \mu_i$). Consequently, $M_R = M - \mu_{int} \approx M$ and the remnant magnetization is apparently symmetric

Scheme 2

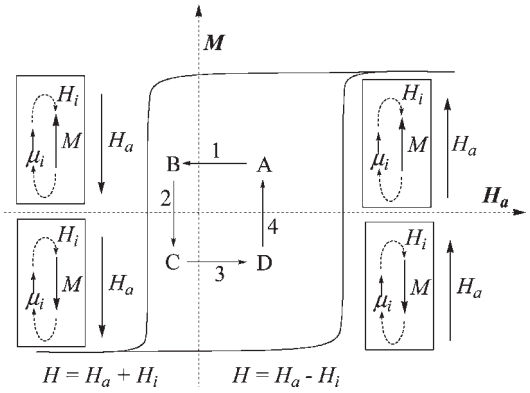

in both branches of the cycle. For $T > 20$ K, μ_i vanish, and the hysteresis loop is symmetric.

Several single crystals and their powder samples (crushed crystals) have been investigated. The asymmetry on the hysteresis loops is a common feature of all the studied single crystals, although the coercive fields can vary significantly from each other. The hysteresis loop of another single crystal at $T = 2.0$ K and under different orientations with respect to the applied magnetic field is shown in the Supporting Information, Figure S10. The coercive field (H_c) for $\alpha = 180°$ is about 5250 G and $H_i = 1250$ G. These values are well above and slightly greater, respectively, than those given in Table 2. Interestingly, the values of the coercive field of the crushed crystals (powdered) are in all the cases greater than the observed ones for any orientation of the single crystal. In this respect, it is interesting to compare Supporting Information, Figure S10a with Supporting Information, Figure S10c as well as Figure 5 (single crystal) with Supporting Information, Figure S7 (the same single crystal but crushed).

The important question at hand is the knowledge about the origin of μ_i. In principle, it could be related to the intrinsic crystal defects, and then the different number of defects occurring in each crystal would account for the different asymmetry and values of the coercive field. Analogously, the number of defects would increase when crushing the crystal and so doing, the values of H_c and H_i would also increase. The presence of these defaults are most likely due to a small deficiency of iron and the charge compensating oxidation process Fe(II) → Fe(III), as well as to some exchange between them (isomorphic substitutions). This could be a source of disorder in the magnetic sublattices. Such a disorder would produce random anisotropies among Fe(II) moments, magnetic frustration and/or weak local spin canting below a given temperature (in our case $T < 20$ K) giving a small, but highly anisotropic, magnetic moment (μ_i).

The phenomenon of asymmetry hysteresis loop is known as the *Exchange Bias* and it refers to a shift of the ferromagnetic hysteresis loop along the field axis by an amount H_{eb} (*exchange bias* field). That is subject of a great interest because of its elusive microscopic origin and its wide technological applications in high-density magnetic recording media, magnetic nonvolatile memories, and spin valve devices. The *exchange bias* is a consequence of an interaction across the interface between dissimilarly ordered magnetic materials, for example, in

the exchange-coupled ferromagnetic (FM)/antiferromagnetic (AFM) systems such as NiFe/NiO,[25] Co/CoO,[26] Fe/MnF_2,[27] CoFe/IrMn bilayers[28] and La−Ca−Mn−O multilayers,[29] and in other motifs.[30] This exchange interaction induces a unidirectional anisotropy as the AF material is cooled through its Néel temperature, T_N. Although it was discovered by Meiklejohn and Bean[31] more than 50 years ago, there has been no satisfactory understanding of the microscopic mechanism of the asymmetric magnetization reversal, the origin of this phenomenon remaining a scientific challenge.[30a]

A deeper study of the magnetic properties of compound **1** is required to get thorough understanding of the origin of the asymmetry on the hysteresis loop. Such an investigation would also clarify *the exchange bias phenomenon*. In that respect, a Mössbauer study as a function of the applied magnetic field and the temperature is planned aiming at observing the magnetic ordering of the sublattices. Analogously, we are investigating the magnetic ordering on the surface of the single crystals by the magneto-optical Kerr effect, the goal being the observation of the domain shapes as well as the occurrence of the oxidation process Fe(II) →Fe(III), which could be more numerous on the surface of the crystal than inside it. In the case where the first top crystal layers were oxidized (Fe^{III} layers), they would be antiferromagnetic, and the crystal could be described as a ferrimagnet surrounded by an antiferromagntic layer. The exchange coupling across the interface of the antiferromagnetic−ferrimagnetic bilayers (exchange-biased) could displace the hysteresis loop along the magnetic field axis.

Compound 2: [$Fe^{III}Mn^{II}$]. The magnetic behavior of **2** differs from that of **1**, in spite of the antiferromagnetic coupling between the neighboring metal ions occurring in both compounds. The magnetic susceptibility measurements of **2** were carried out in the temperature range 2.0−300 K under a *dc* field of 0.1 T. The temperature dependence of χ_m and $\chi_m T$ [χ_m being the magnetic susceptibility per a $Fe^{III}Mn^{II}$ pair] is shown in Figure 7. At 300 K, $\chi_m T$ is equal to 7.67 cm^3 K mol^{-1}, a value which is well below that expected one for a pair of magnetically non-interacting high-spin iron(III) and manganese(II) ions. Upon cooling, $\chi_m T$ continuously decreases, and it attains a minimum value of 3.16 cm^3 K mol^{-1} at 36 K. Below this temperature, $\chi_m T$ exhibits a sharp increase to reach a maximum value of 4.15 cm^3 K mol^{-1} at 32 K, and it further decreases to 0.33 cm^3 K mol^{-1} at 2.0 K. χ_m smoothly increases when cooling from room temperature

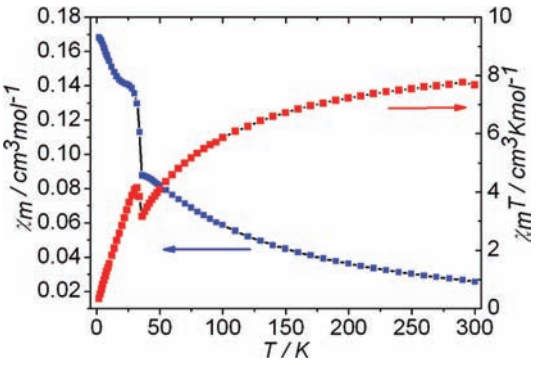

Figure 7. Thermal variation of χ_m and $\chi_m T$ of **2** at 0.1 T.

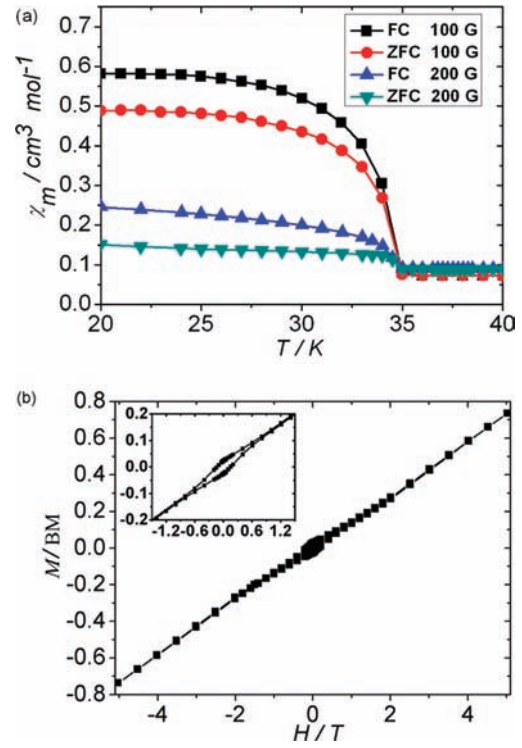

Figure 8. (a) Zero-field-cooled (ZFC) and field-cooled (FC) magnetization curves of **2**. (b) The hysteresis curve of **2** at 2 K.

until 36 K, and then, it exhibits an abrupt increase. The magnetic data of **2** in the temperature range 50−300 K obey the Curie law with the best-fit parameters $C = 8.93$ cm^3 K mol^{-1} and $\theta = -61.11$ K (Supporting Information, Figure S4a). The negative value of θ and the initial decrease of the value of $\chi_m T$ with temperature are due to the antiferromagnetic coupling between the Mn^{II} and Fe^{III} ions. Given that the high-spin Mn^{II} and Fe^{III} ions are spin sextets which have an A_{1g} orbital ground state (in O_h symmetry) with a Landé factor g very close to 2.0, a zero magnetization at saturation will be expected for **2** where the two sublattices are antiparallel. Consequently, the jump of the χ_m and $\chi_m T$ curves below 36 K on cooling is most likely due to a spin canting phenomenon that will be discussed below. Additional support for the occurrence of the canted antiferromagnet behavior in **2** is provided by the field-dependent magnetizations M (H) at 2.0 K also (Supporting Information, Figure S4b and Figure 8b). In the low-temperature region, the zero-field-cooled (ZFC) and field-cooled (FC) magnetization measurements at 100 G (ZFCM/FCM

(25) Liu, Z. Y.; Adenwalla, S. *Phys. Rev. B* **2003**, *87*, 184423.
(26) Radu, F.; Rtzkorn, M.; Schmitte, T.; Siebrecht, R.; Schreyer, A.; Westrholt, K.; Zabel, H. *J. Magn. Magn. Mater.* **2002**, *240*, 251.
(27) Krivorotov, I. N.; Leighton, C.; Nogués, J.; Schuller, I. K.; Dahlberg, E. D. *Phys. Rev. B* **2002**, *65*, 100402(R).
(28) McCord, J.; Schäfer, R.; Mattheis, R.; Barholz, K. U. *J. Appl. Phys.* **2003**, *93*, 5491.
(29) Panagiotopoulos, I.; Moutis, N.; Christidesm, C. *Phys. Rev. B* **2000**, *65*, 132407.
(30) (a) Schlage, K.; Röhlsberger, R.; Klein, T.; Burkel, E.; Strohm, C.; Rüffer, R. *New J. Phys.* **2009**, *11*, 013043. (b) Allende, S.; Escrig, J.; Altbir, D.; Salcedo, E.; Bahiana, M. *Nanotechnology* **2009**, *20*, 445707. (c) Wang, Z.-H.; Habermeier, H.-U.; Cristiani, G.; Sun, J.-R.; Shen, B.-G. *Chin. Phys. Lett.* **2008**, *25*, 278. (d) Iglesias, O.; Batlle, X.; Labarta, A. *J. Magn. Magn. Mater.* **2007**, *316*, 140. (e) Romer, J.; Sort, J.; Hoffmann, A.; García-Martín, J. M.; Dieny, B.; Miranda, R.; Nogués *J. Phys. Rev. Let.* **2005**, *95*, 057204.
(31) Meiklejohn, W. H.; Bean, C. P. *Phys. Rev.* **1957**, *105*, 904.

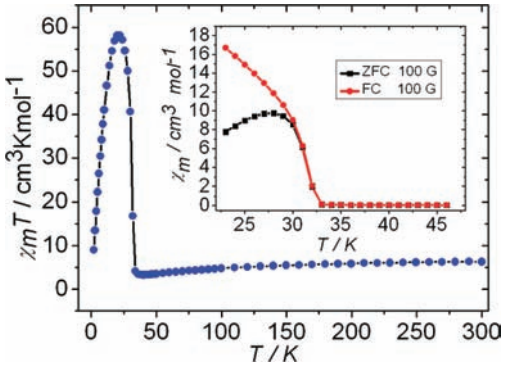

Figure 9. Thermal variation of $\chi_m T$ at 0.1 T. The inset shows the 100 G zero-field-cooled (ZFC) and 100 G field-cooled (FC) magnetization curves of **3**.

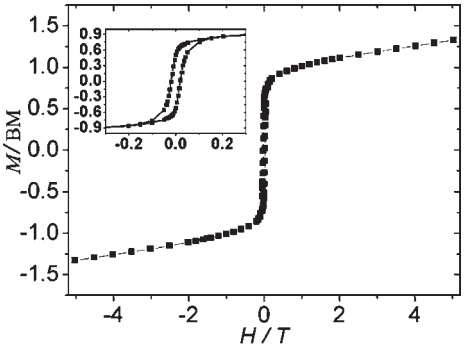

Figure 10. Magnetic hysteresis loops of **3**.

Figure 8a) diverge at 35 K indicating the three-dimensional (3D) long-range antiferromagnetic ordering with weak ferromagnetism, the Néel temperature being 35 K. The *ac* susceptibility H_{dc} = 0 G and H_{ac} = ± 3 G (Supporting Information, Figure S11) further confirm the spin canting in **2**. A hysteresis loop was found in **2** at 2.0 K (Figure 8b), which has a coercive field (H_c) of 1400 G. There are two mechanisms for the spin canting: the antisymmetric exchange (Dzyaloshinsky−Moriya interaction) and the magnetic anisotropy.[23] Usually, Mn^{II} and Fe^{III} ions are practically isotropic, the most likely anisotropy is from second order spin−orbit coupling, which is usually weak. Then for cases like the present one, the Dzyaloshinsky−Moriya (DM) interaction would be responsible for the canting.[13,32] It can proceed through the formato bridge because of the lack of an inversion center in the Fe−(μ-formato)−Mn entity.

A value of canting angle of about 0.06° is easily derived through the saturation value of the magnetization obtained from the 100 G FCM in Figure 8a (0.011 μ_B) and that expected for spin $S = 5/2$ (5 μ_B).[33] The isotropic and antisymmetric exchange in the Fe−(μ-formato)−Mn unit, can be defined by the Hamiltonian $\boldsymbol{H} = J\boldsymbol{S}_{Fe}\boldsymbol{S}_{Mn} + G[\boldsymbol{S}_{Fe} \times \boldsymbol{S}_{Mn}]$.[34] From the Weiss parameter θ = −61 K, a value of $J = 2.4\ cm^{-1}$ can be calculated (the number of nearest neighbors around a magnetic center being $z = 6$).[2] The canting angle (α) is related to the isotropic (J) and antisymmetric (G) exchange parameters through the expression $\tan \alpha = (1/6)^{1/2}(G/J)$ and so, a very small value of $G \approx 6.2 \times 10^{-3}\ cm^{-1}$ can be inferred.[33b]

Compound 3: [$Fe^{III}Co^{II}$]. The magnetic properties of **3** were investigated in the temperature range 2.0−300 K under an applied *dc* field of 0.1 T. They are shown in Figure 9 as $\chi_m T$ versus T plots (χ_m is the magnetic susceptibility per a $Fe^{III}Co^{II}$ pair). At room temperature, $\chi_m T$ for **3** is 6.29 cm^3 K mol^{-1}, which is a value expected for a spin sextet (high-spin Fe^{III}) and a spin quartet (six-coordinated Co^{II}) ions with a significant orbital contribution to the magnetic moment of the cobalt center and assuming a g value of about 2.0.[35] As the temperature decreases, the $\chi_m T$ product slowly decreases to a minimum value of 3.30 cm^3 K mol^{-1} at 40 K, indicating the occurrence of an antiferromagnetic coupling between the adjacent Fe^{III} and Co^{II} ions. Fitting the data in the temperature range 50−300 K with the Curie−Weiss law gives C = 7.64 cm^3 K mol^{-1}, θ = −59.0 K (Supporting Information, Figure S4a). At temperatures below the minimum, $\chi_m T$ exhibits a sharp increase to reach a maximum value of 58.15 cm^3 K mol^{-1} at 22 K, and it further drops to about 9 cm^3 K mol^{-1} at 2.0 K. These features are typical of a ferrimagnetic behavior issuing from the noncompensation of the interacting local spins which are antiferromagnetically coupled. The ferrimagnetic state was confirmed by the isothermal magnetization measurements. The M versus H plots exhibit sharp increases tending to a value of 0.9 μ_B at 0.3 T, and then the values of M increase slowly with the field giving a value of 1.51 μ_B at 5 T (Supporting Information, Figure S4b).

The ZFCM/FCM measurements for **3** were carried out in the temperature range 22−46 K under a dc field of 100 G. The two curves are superposed at higher temperatures (see inset of Figure 9). They increase abruptly below 35 K and then diverge around 30 K indicating long-range magnetic ordering. To further probe the long-range ordering in this compound, *ac* susceptibility measurements of **3** were performed under H_{dc} = 0 G and H_{ac} = 3 G oscillating at 10, 100, and 997 Hz (Supporting Information, Figure S12). They reveal the occurrence of a magnetic phase transition below 33 K because frequency-independent both in-phase χ_m' and out-of-phase χ_m'' signals are observed around this temperature. A peak at 32 K (the Néel temperature), both the in-phase χ_m' and the out-phase χ_m'' components are observed, corresponding to the Néel temperature (Supporting Information, Figure S12). Figure 10 shows the hysteresis loop for a microcrystalline sample of **3**. A small coercive field of 200 G was observed, indicating that **3** is a soft ferrimagnet.

Discussion. Introducing the trivalent iron ions into the niccolite structure framework leads to the formation of three complexes with different magnetism compared with that of the reported complexes[13] $[Me_2en\ H_2^{2+}][M_2(HCOO)_6^{2-}]$ (M = Co and Mn) because two different spins carrier are in the lattices. The magnetism of the complexes can be described as the behavior of two antiferromagnetic coupled sublattices containing different spin carriers Fe^{III} and M^{II}, respectively. The distinct magnetic behaviors in the low temperature are related with the spin carriers of the two sublattices. From the Fe−Mn complex **2** we can see that the magnetic orbitals of Fe(III) ions are same with the

(32) (a) Carlin, R. L.; Van-Duyneveldt, A. J. *Magnetic Properties of Transition Metal Compounds*; Springer-Verlag: New York, 1977. (b) Xu, H.-B.; Wang, Z.-M.; Liu, T.; Gao, S. *Inorg. Chem.* **2007**, *46*, 3089.
(33) (a) Armentano, D.; Mastropietro, T. F.; De Munno, G.; Rossi, P.; Lloret, F.; Julve, M. *Inorg. Chem.* **2008**, *47*, 3772. (b) Armentano, D.; De Munno, G.; Lloret, F.; Palii, A.; Julve, M. *Inorg. Chem.* **2002**, *41*, 2007.
(34) Ferrer, S.; Lloret, F.; Bertomeu, I.; Alzuet, G.; Borrás, J.; Garcia-Granda, S.; Liu-Gonzalez, M.; Haasnoot, J. G. *Inorg. Chem.* **2002**, *41*, 5821.
(35) Lloret, F.; Julve, M.; Cano, J.; Ruiz-Garcia, R.; Pardo, E. *Inorg. Chim. Acta* **2008**, *361*, 3432.

Mn(II) ions, and Fe(III) ion is an isotropic ion too. The magnetism of the three complexes depended on the spin number and anisotropy of M(II) as well as the temperature dependence of sublattices. In **1** the spins of the neighboring ions are 5/2 and 2, which result in a ferrimagnetic state. In **2** the spins of the Fe^{III} and Mn^{II} are all 5/2, and an antiferromagnetic state would be expected. However like the complexes $[CH_3NH_2(CH_2)_2NH_2CH_3^{2+}][M_2(HCOO)_6^{2-}]$, a weak ferromagnetism is presented because the structures, with the non-centrosymmetric bridges of *anti-anti* $HCOO^-$ linking metal sites, satisfy the requirement for the antisymmetric interaction. When the divalent ions changed as Co^{II} in **3** the two antiferromagnetic coupled sublattices are noncompensated leading to a ferrimagnetic state again. Moreover, the orientation to align ordering with the decreasing temperature of the two sublattices in **1** are not the same, leading to the negative value of the magnetizations with small field. In **2** the moments caused by the D-M interaction are the primary reason for spin canting. In the ferrimagnetic state complex **3** no negative value magnetizations was found. As there are no disorders in the structure, the situation might be that the sublattice that contains Co^{II} with smaller saturation magnetization initially orders no quicker with decreasing temperature than the one with the larger saturation magnetization. In fact there are no negative value magnetizations reported in the ferrimagnet $NBu_4Co^{II}[Fe^{II}(ox)_3]$ involving Fe^{III} and Co^{II} as spin carriers, even though in the isomorphic mixed-valent iron complexes show clear negative value magnetizations.[2b,36] $NBu_4Co^{II}[Fe^{II}(ox)_3]$ is a spin glass complex, and no negative value magnetizations are observed. In **3**, for there is no frequency dependence in the ac measurement, the glass behavior was eliminated; however, the peaks are broad not a pointed structure one like that in **1** indicating the transition in **3** is not a single one (Supporting Information, Figures S5 and S12). That may be why no negative value magnetizations were observed in **3**, and the physical origin of that needs further investigation, as well as the asymmetric magnetization reversal observed in the hysteresis loop of **1**.

Acknowledgment. This work was financially supported by the 973 Program of China (2007CB815305), the NNSF of China (20773068 and 21031002) and the Natural Science Fund of Tianjin, China (10JCZDJC22100), and State Key Laboratory of Physical Chemistry of Solid Surfaces, Xiamen University. The Spanish Ministerio de Ciencia y Tecnología through the project Consolider Ingenio CSD2007-00010 ("Nanociencia Molecular"). We also thank Prof. You Song and Zhe-Ming Wang for helpful discussion on the magnetic properties.

Supporting Information Available: X-ray crystallographic data for complexes **1**−**3** in CIF format, Table S1 and Figures S1−S12. These materials are available free of charge via the Internet at http://pubs.acs.org. These materials are available free of charge via the Internet at http://pubs.acs.org.

(36) Bhattacharjee, A.; Feyerherm, R.; Steiner., M. *J. Magn. Mater.* **1999**, *195*, 336.